Micromechanics of actuation of ionic polymer-metal composites

Sia Nemat-Nasser[a)]
University of California, San Diego, Center of Excellence for Advanced Materials, 9500 Gilman Drive, La Jolla, California 92093-0416

(Received 8 October 2001; accepted for publication 3 June 2002)

Ionic polymer-metal composites (IPMCs) consist of a polyelectrolyte membrane (usually, Nafion or Flemion) plated on both faces by a noble metal, and is neutralized with certain counter ions that balance the electrical charge of the anions covalently fixed to the backbone membrane. In the hydrated state (or in the presence of other suitable solvents), the composite is a soft actuator and sensor. Its coupled electrical-chemical-mechanical response depends on: (1) the chemical composition and structure of the backbone ionic polymer; (2) the morphology of the metal electrodes; (3) the nature of the cations; and (4) the level of hydration (solvent saturation). A systematic experimental evaluation of the mechanical response of both metal-plated and bare Nafion and Flemion in various cation forms and various water saturation levels has been performed in the author's laboratories at the University of California, San Diego. By examining the measured stiffness of the Nafion-based composites and the corresponding bare Nafion, under a variety of conditions, I have sought to develop relations between internal forces and the resulting stiffness and deformation of this class of IPMCs. Based on these and through a comparative study of the effects of various cations on the material's stiffness and response, I have attempted to identify potential micromechanisms responsible for the observed electromechanical behavior of these materials, model them, and compare the model results with experimental data. A summary of these developments is given in the present work. First, a micromechanical model for the calculation of the Young modulus of the bare Nafion or Flemion in various ion forms and water saturation levels is given. Second, the bare-polymer model is modified to include the effect of the metal plating, and the results are applied to calculate the stiffness of the corresponding IPMCs, as a function of the solvent uptake. Finally, guided by the stiffness modeling and data, the actuation of the Nafion-based IPMCs is micromechanically modeled. Examples of the model results are presented and compared with the measured data. © *2002 American Institute of Physics.* [DOI: 10.1063/1.1495888]

I. INTRODUCTION

Ionic polymer-metal composites (IPMCs) are soft actuators and sensors. They generally consist of a thin polyelecrolyte membrane of Nafion, Flemion, or Aciplex, plated on both faces by a noble metal, generally platinum or gold or platinum with a layer of finishing gold to improve surface conductivity, and is neutralized with the necessary amount of counter ions, balancing the charge of anions covalently fixed to the backbone membrane. The anions in Aciplex and Nafion are sulfonates, whereas those in Flemion are carboxylates. Figure 1 shows the chemical composition of Nafion and Flemion. When a thin strip of an IPMC membrane in the hydrated state is stimulated by the application of a small (1–3 V) alternating potential, it undergoes a bending vibration at the frequency of the applied voltage, generally no more than a few tens of hertz. Under a suddenly applied step voltage (dc), the composite quickly bends towards the anode. For the Nafion-based IPMCs that are neutralized with metallic cations, the strip then slowly relaxes in the opposite direction, i.e., towards the cathode, while still under the applied voltage. The extent of this backrelaxation depends on the level of hydration and the cation form. For certain cations, e.g., Cs^+ and particularly Tl^+, the backrelaxation is several times greater than the initial fast displacement. If the two faces of this strip are then suddenly shorted, the strip quickly bends further towards the cathode and then slowly relaxes back towards the anode, seldom attaining its original state. The magnitude and speed of these deflections depend on the nature of the counter ions, the structure of the electrodes, the level of hydration (solvent saturation), and other conditions. When the same membrane is suddenly bent, a small voltage of the order of millivolts is produced across its faces. Hence, these IPMCs are soft actuators and sensors; see, e.g., Refs. 1 and 2.

For some large organic cations, e.g., tetrabutylammonium (TBA), a slow deflection towards the anode is observed under an applied step voltage, for both the Nafion- and Flemion-based composites. For small organic cations, e.g., tetramethylammonium (TMA), both a fast motion and a slow backrelaxation are observed for the Nafion-based IPMC, but not for the Flemion-based composite. Indeed, preliminary

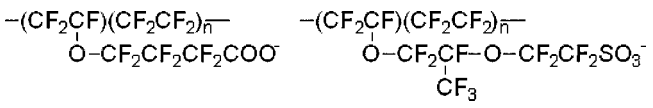

FIG. 1. Chemical structure of Flemion (left), and Nafion (right).

[a)]Electronic mail: sia@ucsd.edu

observation of the step-voltage actuation of a Flemion-based IPMC with purely gold electrodes shows that the initial fast displacement of the cantilevered strip towards the anode is always followed by a slow relaxation in the same (i.e., towards the anode) direction for both metallic and organic cations. Hence, unlike for the Nafion-based composites, no backrelaxation has been detected in these preliminary experiments for the Flemion-based IPMCs that are actuated by the application of a step voltage.[3]

Nemat-Nasser and Thomas[4] have examined various aspects of the Nafion-based composites and their actuation and sensing properties, providing some detailed discussion of the potential micromechanisms and models to simulate them. In my laboratories at the University of California, San Diego we have been carrying out a systematic experimental evaluation of the response of both metal-plated and bare Nafion and Flemion in various cation forms and at different hydration levels. Based on the results of the measured stiffness and actuation of the material under a variety of conditions, I have developed certain relations between internal forces and the resulting stiffness and deformation of this class of IPMCs. I have sought to decipher potential micromechanisms responsible for the complex electromechanical behavior of these materials. Some of these results are summarized in the present article. For an overview of recent developments and applications of IPMCs, and for references, see Ref. 4.

II. MICROSTRUCTURE AND PROPERTIES

A. Composition and properties

IPMCs considered in the present work are made from Nafion 117 (i.e., 1,100 g per mole sulfonate dry membrane of 178 μm thickness). The metal-plated composites are about 200-μm-thick membranes, consisting of the following constituents:

(1) backbone perfluorinated copolymer of polytetrafluoroethylene with perfluorinated vinyl ether sulfonate pendants, forming interconnected nanoscale clusters that contain the sulfonates and their neutralizing cations;
(2) electrodes consisting of 3–10 nm in diameter metal (generally platinum) particles, distributed mainly within 10–20 μm depth of both faces of the membrane, and usually covered with 1–5 μm gold plating;
(3) neutralizing cations; and
(4) a solvent, usually water.

The response of the IPMC depends on the nature of the backbone polymer, the structure of the electrodes, the counter ions, and the level of hydration. Figure 2(a) shows various constituents in a typical cross section of an IPMC with Nafion as its backbone polymer, indicating the microstructure of the electrode region [insert A in Figs. 2(a) and 2(b)] and the cluster morphology of the polymer [insert B in Figs. 2(a) and 2(c)]. The density of the metal particles decreases with depth and generally is very small at the center of the strip. Figure 2(c) is a high-resolution transmission electron microscopy (TEM) of the central portion of an IPMC, showing sparsely distributed platinum particles and the clustering of the polymer (see Refs. 5 and 6 for further information on bare Nafion).

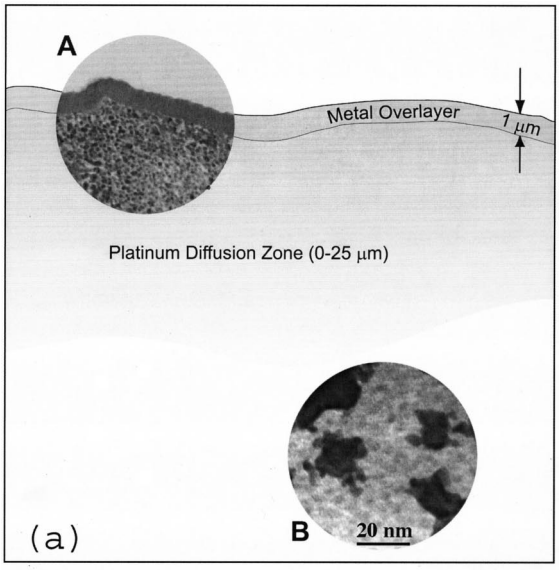

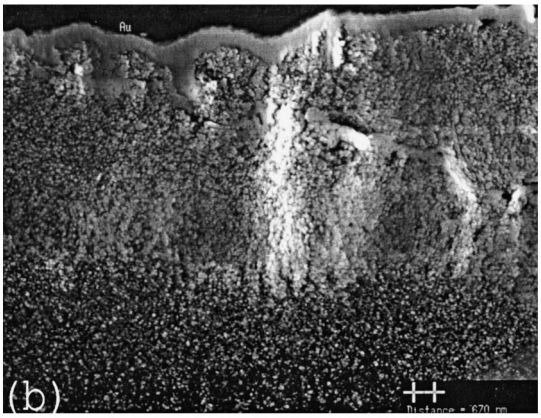

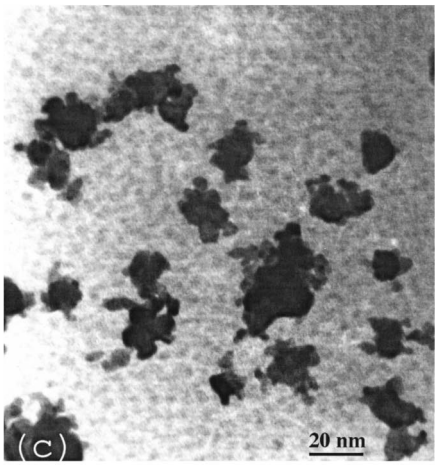

FIG. 2. (a) Cross section of a typical Pt/Au-plated Nafion 117, showing the morphology of the electrode zone (insert A) and polyelectrolyte membrane (insert B); (b) Electrode structure of Pt/Au-plated Nafion 117; distance between crosses is 670 nm; and (c) high-resolution TEM of the central portion of a Pt-plated Nafion 117, showing some Pt particles (dark) and a cluster morphology of the polymer.[7]

The metal plating process can be adjusted to control the

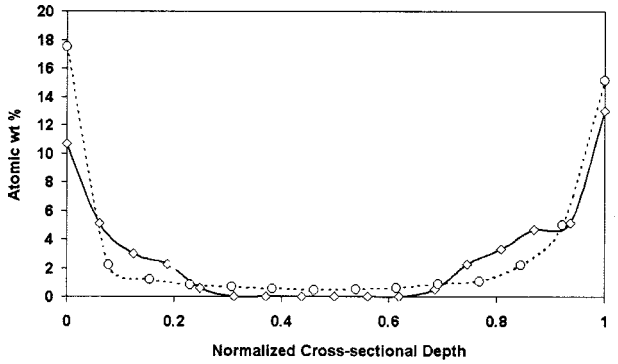

FIG. 3. Distribution of platinum particles over the thickness of two Nafion-based IPMCs.[15]

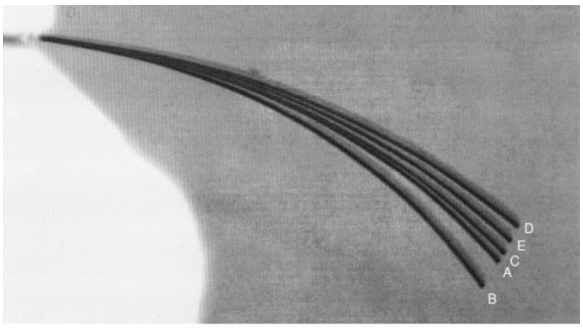

FIG. 4. Actuation of a K^+-form Nafion-based IPMC under 1 V dc; from A to B fast initial motion, from B to C slow relaxation, from C to D fast motion upon shorting, and from D to E slow final relaxation.[3]

size and distribution of the metal particles,[8–11] which in turn affect the response of the composite in a major way. Platinum distribution for two examples is shown in Fig. 3, using energy dispersive x-ray spectroscopy. The metal plating for these samples has been preformed by Shahinpoor and Kim.[12,13] The sample corresponding to the dashed curve contains finer and more extensively distributed platinum particles, has greater capacitance, and shows better actuation than the other sample (solid curve). The Flemion-based IPMCs that have been tested have pure gold electrodes with a dendritic structure.[14]

For the neutralizing cations, we have used H^+, Li^+, Na^+, K^+, Rb^+, Cs^+, Ti^+, Ba^{++}, and several organic cations such as TBA^+ and TMA^+. Remarkably, the stiffness of the bare polymer as well as that of the corresponding IPMC changes with the cation type for the same membrane and at the same level of solvent uptake (e.g., hydration), as well as with the degree of solvent uptake. The amount of solvent uptake at full saturation depends on the cation used, being a maximum for H^+. It also depends on the temperature and duration of the solvent-uptake process. In what follows attention is focused on water as the solvent.

B. Actuation and sensing

A Nafion-based IPMC sample in the hydrated state performs an oscillatory bending motion when an alternating voltage is imposed across its faces, and it produces a voltage when suddenly bent. When the same strip is subjected to a suddenly imposed and sustained constant voltage (dc) across its faces, an initial fast displacement (towards the anode) is generally followed by a slow relaxation in the reverse direction (towards the cathode), particularly in an aqueous environment. If the two faces of the strip are then shorted during this slow relaxation towards the cathode, a sudden fast motion in the same direction (towards the cathode) occurs, followed by a slow relaxation in the opposite direction (towards the anode). Figure 4 illustrates these processes for a K^+-form Nafion-based IPMC. The magnitudes of the two fast motions and the backrelaxation that follows the fast motions change with the cation used.

More recent experiments using ethylene glycol or glycerol as solvents have shown drying of the anode face and wetting of the cathode face of the strip, during the entire deformation process under an applied dc voltage. Indeed, solvent droplets appear on the cathode face after the bending relaxation towards the cathode has advanced, while the anode face continues to remain dry. Once the two faces of the IPMC are shorted, the droplets disappear, diffusing back into the composite. In addition, measurement of the current flow during the initial fast motion towards the anode and subsequent relaxation towards the cathode shows continued migration of cations into the cathode region even when this region is undergoing contraction. With water as the solvent, the slow backrelaxation is smallest for the Li^+-form and greatest for the Tl^+-form cation, among the cations we have tested. For large hydrophobic organic cations such as TBA^+, a slow motion towards the anode is observed with no backrelaxation. Remarkably, and in contrast to the response of the Nafion-based composites, the fast and the following slow relaxation motions of the Flemion-based IPMCs that we have tested in the metallic cation forms are in the same direction. That is, when the dc voltage is imposed, both the initial fast motion and the following slow relaxation are towards the anode, and then, upon shorting, they are both towards the cathode. This difference in the response may in part be attributed to the difference in the acidity (pK_a) of the sulfonates (e.g., about -5.1 for trifluoromethanesulfonic acid, CF_3SO_3H, triflate) in the Nafion-based IPMCs, as compared with that of carboxylates (e.g., about 0.23 for trifluoroacetic acid, CF_3COOH) in the Flemion-based IPMCs. Also, the electrode structure and composition of the two IPMCs are quite different, affecting the corresponding response.

The objective is to identify the underpinning micromechanisms responsible for each response, quantify these mechanisms mathematically, and, in this manner, develop physics-based predictive models that describe the observed phenomena for various ion-form IPMCs.

C. Micromechanisms of actuation

In an IPMC, the backbone fluorocarbon polymer is hydrophobic and the anions (sulfonates for the Nafion-based, and carboxylates for the Flemion-based IPMCs) are hydrophilic, resulting in the formation of clusters, within which the anions and their neutralizing cations are concentrated. The anions (sulfonates or carboxylates) within the clusters are

covalently attached to the fluorocarbon matrix, while in a hydrated state the associated unbound cations can move within the water that permeates the interconnected clusters.[5,16–24] In the absence of an applied voltage, the cations and anions form conjugate pairs, with the cations optimally distributed within each cluster to minimize the overall energy. Each cation-anion pair may be visualized as a pseudo-dipole whose effective moment depends on the nature of the cation and the number of available water molecules. For the sake of referencing, in the present work, we choose to identify each cation-anion conjugate pair as a dipole, even though they do not form a true dipole. Indeed, even for the same cation, the distance between the two charges corresponding to such a pseudo-dipole depends on the level of hydration and, hence, is a function of water uptake. This fact will be incorporated into the model, as is explained later on in the present work.

An applied electric field affects the cation distribution within the membrane, forcing the cations to migrate towards the cathode. This change in the cation distribution produces two thin layers, one near the anode and another near the cathode boundaries. We refer to these as anode and cathode boundary layers, respectively. The clusters within the anode boundary layer are depleted of their cations, while clusters within the cathode boundary layer are cation rich. Nemat-Nasser and Thomas[4] discuss potential effects that such changes in the cation concentration may produce within these boundary layers. A summary of their comments is given first. Then, the most significant effects are examined, modeled mathematically, and their influence on the actuation of the composite is discussed and illustrated.

At the anode and cathode boundary layers, the respective reduction and increase in the concentration of the ions may produce any of the following effects.

(1) A decrease in the effective stiffness of the polymer in the anode, and an increase in this stiffness in the cathode boundary layer, respectively.
(2) A repulsive electrostatic force among the fixed anions of each cation-depleted cluster in the anode boundary layer, which tends to increase the average cluster volume and also relax the prestretched polymer chains between adjacent clusters, increasing their entropy and decreasing their elastic energy. In the clusters within the cathode boundary layer, the additional cations initially repel the existing cation-anion pseudo-dipoles, contributing to the rapid expansion of these clusters and hence the fast bending motion of the IPMC towards the anode. In time the cations in the cathode boundary layer may slowly be redistributed under the influence of the strongly acidic sulfonates, producing the slow back-relaxation motion of the Nafion-based IPMCs (but not necessarily the Flemion-based IPMCs that contain the weakly acidic carboxylates).
(3) Reorientation of the water molecules in the clusters, which tends to increase the effective electric permittivity of the clusters in the anode, and decrease it in the clusters within the cathode boundary layer. This in turn reduces (increases) the electrostatic interaction forces among the charges within each cluster of the anode (cathode) boundary layer.
(4) Removal from the anode and addition to the cathode boundary layer clusters, water molecules by cation migration, which tend to quickly change the clusters' average volume. [For the H^+ cations, however, there is no water removal from or addition to the clusters by this mechanism, since H^+ migrates via the Grotthuss or hopping mechanism.[25–27] Indeed, the removal (addition) of H^+ ions actually increases (decreases) the volume of the water within the corresponding clusters, due to the electrostriction effects on the proton hydration shells. Furthermore, the hydrophobic organic cations do not necessarily transport water as they redistribute].
(5) A change (decrease for the anode and increase for the cathode boundary layer) in the osmotic pressure in the clusters, due to the change in the ion concentration.

Effect (1) relates to the fact that anion-cation coupling within the clusters provides a pseudo cross-linking and a structured arrangement with concomitant increase in the internal energy and decrease in the entropy of the system. While the phenomenon may be modeled based on certain assumptions,[24] its experimental verification presents major difficulties. On the other hand, effects (2)–(5) can be modeled directly and indeed do explain the observed behavior of the IPMCs, as is shown in what follows.

D. Some basic characteristic parameters

One of the most important parameters that characterizes an ionomer, is its ion content, which is operationally defined by its equivalent weight, EW_{ion}. For Nafion 117 in the H^+-form, $EW_{H+} = 1100$ g dry sample per mole SO_3^- ion. It is convenient to extend this definition to IPMCs in various cation forms, as follows:

$$EW_{ion} = \frac{EW_{H+} - 1.008 + FW_{ion}}{SF}, \tag{1}$$

where FW_{ion} is the formula weight of the cation used, and SF is a scaling factor that measures the mass fraction of the added metal electrodes, SF = mass of dry backbone ionomer per unit mass of dry IPMC. For bare samples (no metal electrodes), SF = 1. When the areal densities of the backbone polymer and the added metal electrodes are both constant, then SF, is also constant.

Another important parameter is the hydration, defined by the water uptake, w, which is the volume of water absorbed, V_{H_2O}, divided by the dry volume, V_{dry}, of the IPMC:

$$w = \frac{V_{H_2O}}{V_{dry}}. \tag{2}$$

From the earlier two parameters, we calculate the anion molality, m, within the sample

$$m = 10^3 \frac{\rho}{EW_{ion} w}. \tag{3}$$

This measures moles of anion within the IPMC per liter of its water content. In Eq. (3), ρ is the dry density of the IPMC membrane, measured in g/cm^3. The number of moles of anion per cubic meter of the hydrated sample and the anion charge density in Coulomb per cubic centimeter (C/cm^3) of the dry sample then, respectively, are

$$\mathrm{C}^- = 10^3 \frac{w}{1+w} m, \quad \mathrm{Q}_{\mathrm{dry}} = \frac{\rho F}{\mathrm{EW}_{\mathrm{ion}}}, \tag{4}$$

where F is Faraday's constant (96 487 C/mol). Hence, the total ion concentration, c, measured as mole anion and cation per mole water, and the associated total molality, νm, are

$$c = 18\times 10^{-6}(\mathrm{C}^+ + \mathrm{C}^-)\frac{1+w}{w},$$

$$\nu \mathrm{m} = 10^{-3}(\mathrm{C}^+ + \mathrm{C}^-)\frac{1+w}{w}, \tag{5}$$

where C^+ is the concentration of cations measured in mole per cubic meter of hydrated sample.

III. STIFFNESS VERSUS HYDRATION

A. Stress field in polymer matrix

A dry sample of a bare polymer or an IPMC in an aqueous environment absorbs water until the resulting pressure within its clusters is balanced by the elastic stresses that are consequently developed within its backbone polymer membrane. From this observation the stiffness of the membrane can be calculated as a function of the water uptake for various cations. We first consider the balance of the cluster pressure and the elastic stresses for the bare polymer (no metal plating) and then use the results to calculate the stiffness of the corresponding IPMC by including the effect of the added metal electrodes. The procedure also provides a way of estimating many of the microstructural parameters that are needed for the modeling of the actuation of the IPMCs. Since, for the Nafion-based IPMCs, the overall stiffness of both the bare membrane and the corresponding IPMCs has been measured directly as a function of the hydration,[15] the basic assumptions and the results can thus be subjected to experimental verification.

The stresses within the backbone polymer may be estimated by modeling the polymer matrix as an incompressible elastic material.[28,29] Here, it will prove adequate to consider a neo-Hookean model for the matrix material. In this model, the principal stresses, σ_I, are related to the principal stretches, λ_I, by

$$\sigma_I = -p_0 + K\lambda_I^2, \tag{6}$$

where p_0 is an undetermined parameter (pressure) to be calculated from the boundary data; in spherical coordinates, $I = r, \theta, \varphi$, for the radial and the two hoop components; and K is an effective stiffness which depends on the cation type and its concentration, and on the water uptake, w.

The aim is to calculate K and p_0 as functions of w for various ion-form membranes. To this end, we examine the deformation of a unit cell of the hydrated polyelectrolyte (bare membrane) by considering a spherical cavity of initial (i.e., dry state) radius a_0 (representing a cluster), embedded at the center of a spherical matrix of initial radius R_0, and placed in a homogenized hydrated membrane, referred to as the matrix. We assume that the stiffness of both the spherical shell and the homogenized matrix is the same as that of the (yet unknown) overall effective stiffness of the hydrated membrane. For an isotropic expansion of a typical cluster, the two hoop stretches are equal, $\lambda_\varphi = \lambda_\theta$. From incompressibility $\lambda_r \lambda_\theta^2 = 1$, and Eq. (6) yields

$$\sigma_r(r_0) = -p_0 + K\lambda_\theta^{-4}(r_0),$$

$$\sigma_\theta(r_0) = -p_0 + K\lambda_\theta^2(r_0), \tag{7}$$

where r_0 measures the initial radial length from the center of the cluster. We assume that the effective elastic resistance of the (homogenized hydrated) membrane balances the cluster's pressure, p_c, which is produced by the combined osmotic and electrostatic forces within the cluster.

Denote the initial porosity (volume of voids divided by total volume) by n_0. Then, the initial void ratio (void volume divided by volume of dry polymer) is $w_0 = n_0/(1-n_0)$. Both n_0 and w_0 are very small, i.e., $(n_0, w_0) \ll 1$. Consider cases where the water uptake is suitably large, i.e., cases where $w > w_0$. Then, with a denoting the cluster radius and R is the outer radius of the representative spherical shell, both after water uptake, obtain

$$n_0 = (a_0/R_0)^3, \quad w_0 = \frac{n_0}{1-n_0},$$

$$w = \frac{n_0}{1-n_0}\lambda_\theta^3(a_0) = \frac{\lambda_\theta^3(R_0)}{1-n_0} - 1, \tag{8}$$

where $\lambda_\theta(a_0) = a/a_0$ and $\lambda_\theta(R_0) = R/R_0$ are the hoop stretches at the cluster surface and at $r_0 = R_0$, respectively. Upon deformation, material points initially at r_0 move to r:

$$r^3 = r_0^3 + a_0^3(w/w_0 - 1), \tag{9}$$

where Eq. (8) is used. The radial and hoop stresses at an initial distance of r_0 from the cluster center are

$$\sigma_r(r_0) = -p_0 + K[(r_0/a_0)^{-3}(w/w_0 - 1) + 1]^{-4/3},$$

$$\sigma_\theta(r_0) = -p_0 + K[(r_0/a_0)^{-3}(w/w_0 - 1) + 1]^{2/3}. \tag{10}$$

The radial stress, σ_r, must equal the pressure, p_c, in the cluster, at $r_0 = a_0$. In addition, the volume average of the stress tensor, taken over the entire membrane, must vanish in the absence of any externally applied loads. This is a consistency condition that to a degree accounts for the interaction among clusters. These conditions are sufficient to yield the undetermined pressure, p_0, and the stiffness, K, in terms of w and w_0, for each ion-form bare membrane, as is discussed in what follows.

B. Pressure in clusters

For the hydrated bare membrane or an IPMC in the M^+-ion form, and in the absence of an applied electric field, the pressure within each cluster, p_c, consists of osmotic, $\Pi(\mathrm{M}^+)$, and electrostatic, p_{DD}, components

$$p_c = \Pi(\mathrm{M}^+) + p_{\mathrm{DD}}, \tag{11}$$

where the electrostatic component is produced by the ionic interaction that we represent by dipole–dipole interaction forces (hence, the subscript DD), approximating cation-anion conjugate pairs as dipoles.

1. Osmotic pressure

The osmotic pressure is calculated by examining the difference between the chemical potential of the free (bath) water and that of the water within a typical cluster of known ion concentration within the membrane. The chemical potential of water within the membrane (measured per mole) is expressed as

$$\mu^w=\mu_0^w+18\times10^{-6}p+RTg\ln\left(\frac{1}{1+c}\right)$$
$$=\mu_0^w+18(10^{-6}p-10^{-3}RT\phi\nu m), \tag{12}$$

where g is the ''rotional'' and ϕ is the ''practical'' osmotic coefficient, being related by $g=(1+0.009\nu m)\phi$; $\nu=2$; and p is the water pressure in pascal. The osmotic coefficient $\phi(m)$ depends on the molality, m.[30] The osmotic pressure in mega pascal, associated with the cation M^+, is now obtained from the difference in the chemical potential of the cluster water and the free bath water. This gives

$$\Pi(M^+)=\frac{\nu\rho RT\phi}{EW_{ion}w}=\frac{\nu Q_{dry}^- K_0\phi}{w},\quad K_0=\frac{RT}{F}, \tag{13}$$

where Q_{dry}^- is defined in Eq. (4).

2. Dipole–dipole interaction pressure

Consider now the electrostatic interaction forces within a typical cluster. In the dry state, and in the absence of an applied electric field, the cations, M^+'s, and the sulfonates, SO_3^-'s, form pseudo-dipoles that are distributed over the cluster surface. In a hydrated state, the hydration water molecules intervene and modify the strength of these dipoles and their interaction forces. Depending on the water content, the electrostatic interaction may produce hydrostatic tension or compression within the clusters. Their effective moments depend on the water content and change with the water uptake, w.

To estimate the pressure p_{DD}, produced by the electrostatic forces in a typical cluster, consider a sphere of radius a, containing radial dipoles of density $p=\alpha q$, uniformly distributed over the sphere's surface area. Here, q is the charge density and $\alpha=\alpha(w)$ is an effective dipole length, a function of the water uptake, w. The radial pressure on the sphere is then calculated by integrating the Coulomb forces acting on the dipoles of an elementary surface area, due to all other dipoles that are distributed over the sphere. This gives

$$p_{DD}=\frac{3!p^2}{2\kappa_e a^2}=\frac{3q^2\alpha^2}{\kappa_e a^2}, \tag{14}$$

where $\kappa_e=\kappa_e(w)$ is the effective electric permittivity in the cluster, which changes with the water uptake, w. Since anions reside solely within the clusters, the surface charge density, q, can be calculated as follows:

$$q=Q_B^-\frac{4\pi}{3}(R_0^3-a_0^3)\frac{1}{4\pi a^2}=Q_B^-\frac{4\pi}{3}(R^3-a^3)\frac{1}{4\pi a^2}$$
$$=\frac{Q_B^-}{3w_0}\frac{a_0}{\lambda_\theta^2(a_0)}\approx\frac{Q_B^-}{3}\frac{R_0}{w^{2/3}},\quad Q_B^-=\frac{\rho_B F}{EW_{ion}}, \tag{15}$$

where Q_B^- is the anion charge density (in C/cm^3) of the dry bare membrane, ρ_B is the dry density of the bare membrane, and EW_{ion} is its equivalent weight. The last expression is obtained using the incompressibility of the polymer and the fact that $(n_0,w_0)\ll1$. Now, in view of Eqs. (8) and (15), expression (14) reduces to

$$P_{DD}=\frac{1}{3\kappa_e}Q_B^{-2}\frac{\pm\alpha^2}{w^2}. \tag{16}$$

Here, the plus sign is for repulsive, and the minus sign is for attractive dipole–dipole interaction forces. From Eqs. (13) and (16), the cluster pressure finally becomes

$$p_c=\frac{\nu Q_B^- K_0\phi}{w}+\frac{1}{3\kappa_e}Q_B^{-2}\frac{\pm\alpha^2}{w^2}. \tag{17}$$

C. Stiffness of bare ionomer versus hydration

We now estimate the overall effective stiffness, $K=K(w)$, and pressure, $p_0=p_0(w)$, as functions of the water uptake, w, for the bare ionomer. To this end, observe that the radial stress, $\sigma_r(r_0)$, at $r_0=a_0$, must balance the common pressure, p_c, in the (interconnected) clusters

$$\sigma_r(a_0)=-p_c. \tag{18}$$

To account for the interaction among the clusters, and to ensure consistency, the volume average of the stress tensor must vanish in the absence of an external load. This requirement yields two equations. The first shows that the volume average of the deviatoric part of the stress tensor taken over the dry polymer matrix only (i.e., excluding the clusters) must vanish. The second relates the volume average of the spherical part of the stress tensor (taken again over the dry polymer matrix) to the cluster pressure, p_c, as follows:

$$\frac{1}{V_{dry}}\int_{V_{dry}}\tfrac{1}{3}(\sigma_r+2\sigma_\theta)dV_{dry}-wp_c=0. \tag{19}$$

The integral can be evaluated in closed form for a typical unit cell with spherical shell of thickness R_0-a_0, and using Eq. (10), we obtain

$$-p_0+Kw_0I_n=wp_c,$$
$$I_n=\frac{1+2An_0}{n_0(1+An_0)^{1/3}}-\frac{1+2A}{(1+A)^{1/3}},$$
$$A=\frac{w}{w_0}-1. \tag{20}$$

Combining Eqs. (17), (18), and $(20)_1$, we now arrive at

$$K=p_c\frac{(1+w)}{w_0I_n-\left(\frac{w_0}{w}\right)^{4/3}},$$

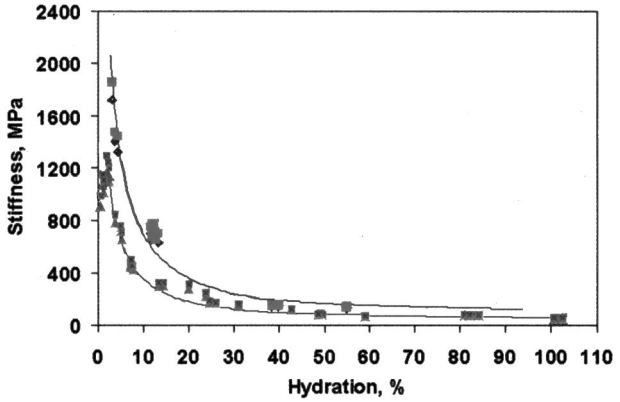

FIG. 5. Uniaxial stiffness (Young's modulus) of bare Nafion 117 (lower data points and the solid curve, model) and an IPMC (upper data points and the solid curve, model) in the Li^+ form vs hydration water, w.

$$p_0 = K\left(\frac{w}{w_0}\right)^{-4/3} + p_c. \tag{21}$$

D. Comparison with experimental data

In a series of experiments, the extensional Young's modulus, Y, of strips of bare Nafion 117 in various ion forms, is measured as a function of the water uptake, w.[15] These results are now used to check the model and, more importantly, to fix the model parameters. Since both the polymer matrix and water can be regarded as incompressible at the level of the involved stresses, the hydrated composite can be regarded as incompressible when the water uptake is fixed; i.e., in the absence of water exchange with the surrounding environment, the hydrated membrane is assumed to be incompressible. For small axial strains (i.e., less than 1%), therefore, the Young modulus Y_B of the hydrated strip of bare polymer relates to the stiffness K, by

$$Y_B = 3K, \tag{22}$$

which follows directly from Eq. (6) for small strains. Figure 5 shows the experimentally measured Y_B for Li^+-ion form Nafion 117. The measurement technique and the associated instruments are discussed elsewhere.[15] Here we use the data to check our model results, as follows.

In Fig. 5, the lower solid curve is obtained from Eq. $(21)_1$, in the following manner. For the purposes of calculation, we use an initial porosity of $n_0 = 0.01$, which is rather large but suitable in the present context. Then we calculate EW_{Li^+} from Eq. (1) with FW_{Li^+} equal to 6.94 for Li^+. Since the bare Nafion is used SF is equal to 1. For the value of the osmotic factor, ϕ, we use 1, although $\phi = 1.6$ may be inferred from the data reported in the literature for metal salts of Li^+ with trifluoromethanesulfonic acid (CF_3SO_3H, triflate).[31] In view of the uncertainty in the values of several other involved parameters, $\phi = 1$ is justified. The dry density ρ_B, is measured to be about 2.01 g/cm^3. With $\nu = 2$, $R = 8.3$ J/mol/K, and $T = 300$ K for room temperature, the only unknown quantity in Eq. (17) and, hence, in Eq. $(21)_1$ is the ratio α^2/κ_e. To estimate κ_e as a function of the water uptake, w, note that water molecules are polar. As part of the hydration shell of an ion, water has a dielectric constant of only 6, whereas as free molecules, its dielectric constant is about 78 at room temperature. The static hydration shell of Li^+ is about 6, which equals its corresponding coordination number, CN; see Nemat-Nasser and Thomas[4] for comments. Let m_w be the number of mole water per mole ion (cation and anion) within a cluster, and note that

$$m_w = \frac{EW_{ion} w}{18 \nu \rho_B}. \tag{23}$$

Hence, when the water uptake is less than CN moles per mole of ion within a cluster, we set $\kappa_e = 6\kappa_0$, where $\kappa_0 = 8.85 \times 10^{-12}$ F/m is the electric permittivity of the free space. On the other hand, when more water is available in a cluster, i.e., when $m_w > CN$, we calculate $\kappa_e = \kappa_e(w)$, as follows:

$$\kappa_e = \frac{7+6f}{7-6f} 6\kappa_0, \quad f = \frac{m_w - CN}{m_w}. \tag{24}$$

Expression $(24)_1$ is obtained from Eq. (B5) of Appendix B Ref. 24 by setting $\kappa_1 = 6\kappa_0$ and $\kappa_2 = 78\kappa_0$ in

$$\kappa_e = \frac{\kappa_2 + \kappa_1 + f(\kappa_2 - \kappa_1)}{\kappa_2 + \kappa_1 - f(\kappa_2 - \kappa_1)} \kappa_1.$$

Note that Eq. (44) of Ref. 24 and Eq. (34) of Ref. 4 contain typographical errors, while Eq. (B5) Ref. 24 is correct. These authors use a micromechanical model to obtain their result; see Ref. 32.

We now calculate the parameter $\pm\alpha^2$, as follows. As a first approximation, we let α^2 vary linearly with w for $m_w \leqslant CN$, i.e., we set

$$\pm\alpha^2 = a_1 w + a_2, \quad \text{for } m_w \leqslant CN, \tag{25}$$

and estimate the coefficients a_1 and a_2 from the experimental data. For $m_w > CN$, furthermore, we assume that the distance between the two charges forming a pseudo-dipole is controlled by the effective electric permittivity of the their environment (i.e., water molecules), and hence, is given by

$$\alpha = 10^{-10} \frac{7+6f}{7-6f} (a_1 w + a_2)^{1/2}; \tag{26}$$

note that for $m_w > CN$, we have $a_1 w + a_2 > 0$. The lower solid curve in Fig. 5 corresponds to the values $a_1 = 1.728$ and $a_2 = -0.0778$ which are obtained by setting $Y_B = 1250$ for $w = 0.02$ and $Y_B = 60$ for $w = 1.00$. Parameters a_1 and a_2 are thus empirically fixed in this model.

E. Stiffness of IPMC versus hydration

In Fig. 5 the upper data points represent the measured stiffness of a Nafion-based IPMC in the Li^+ form, as a function of its hydration.[15] The upper solid curve is the model result obtained using the model (lower solid curve in the figure) for the bare Nafion in the Li^+ form, as follows.

The gold plating is about 1 μm layer on both faces of an IPMC strip, while platinum particles are distributed through the first 10–20 μm surface regions, with diminishing density [see Figs. 2(a) and 2(b)]. To include the effect of these metal

electrodes on the overall stiffness of the composite, we assume a uniaxial stress state and average over the strip's volume to obtain the average strain and stress, as follows:

$$\overline{\varepsilon}_{\mathrm{IPMC}}=f_{MH}\overline{\varepsilon}_M+(1-f_{MH})\overline{\varepsilon}_B,$$

$$\overline{\sigma}_{\mathrm{IPMC}}=f_{MH}\overline{\sigma}_M+(1-f_{MH})\overline{\sigma}_B,\quad f_{MH}=\frac{f_M}{1+w},\tag{27}$$

where the barred quantities are the average values of the strain and stress in the IPMC, bare (hydrated) membrane, and metal electrodes, respectively; and f_M is the volume fraction of the metal plating in a dry sample, given by

$$f_M=\frac{(1-\mathrm{SF})\rho_B}{(1-\mathrm{SF})\rho_B+\mathrm{SF}\rho_M},\tag{28}$$

where $\rho_M=20$ g/cm^3 is the mass density of the metal plating and SF is the scaling factor, representing the weight fraction of dry polymer in IPMC. We assume that the average stress in the bare polymer and in the metal are given by

$$\overline{\sigma}_B=A_B\overline{\sigma}_{\mathrm{IPMC}},\quad \overline{\sigma}_M=A_M\overline{\sigma}_{\mathrm{IPMC}},\tag{29}$$

where A_B and A_M are the concentration factors, giving the average stress in the bare polymer and metal in terms of the average stress of the IPMC, $\overline{\sigma}_{\mathrm{IPMC}}$. Setting $\overline{\sigma}_B=Y_B\overline{\varepsilon}_B$, $\overline{\sigma}_M=Y_M\overline{\varepsilon}_M$, and $\overline{\sigma}_{\mathrm{IPMC}}=\overline{Y}_{\mathrm{IPMC}}\overline{\varepsilon}_{\mathrm{IPMC}}$, it follows from Eqs. (27), (28), and (29) that

$$\overline{Y}_{\mathrm{IPMC}}=\frac{Y_MY_B}{BA_BY_M+(1-BA_B)Y_B},$$

$$B=\frac{(1+\overline{w})(1-f_M)}{1+\overline{w}(1-f_M)},\quad w=\overline{w}(1-f_M).\tag{30}$$

Here Y_B is evaluated at hydration of $\overline{w}$ when the hydration of the IPMC is w. The latter is measured directly at various hydration levels, as shown in Fig. 5 for an IPMC in the Li^+ form. Since most IPMCs that we have studied contain both platinum (with 21.45 g/cm^3 mass density) and gold (with 19.3 g/cm^3 mass density), ρ_M in Eq. (28) represents their combined overall density. The quantity SF can be measured directly[4] or indirectly from the measured density of the IPMC in various ion forms.[15] For the data shown in Fig. 5, $\rho_M=20$ g/cm^3, $\rho_B=2.0$ g/cm^3, and SF$=0.60$, resulting in $f_M=0.0625$. For Y_M we have used 75 GPa and for the concentration factor we have used $A_B=0.50$. Then, for each value of w the corresponding value for the bare polymer, given by the lower solid curve in Fig. 5, is entered into Eq. $(30)_1$ to obtain the associated value for the upper solid curve. Similar results are obtained for other IPMCs in other ion forms, as illustrated for the Rb^+-form IPMC in Fig. 6. Other data are presented elsewhere.[15]

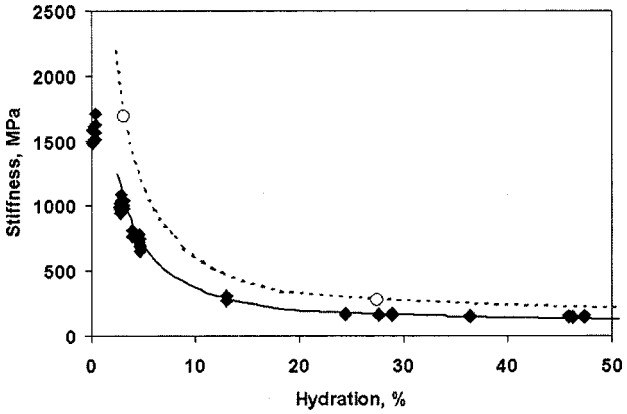

FIG. 6. Uniaxial stiffness (Young's modulus) of bare Nafion 117 (lower data points and the solid curve, model) and an IPMC (upper two open circles and the dotted curve, model) in the Rb^+ form vs hydration water; FW$=85.5$, $\rho_B=2.10$, $a_1=2.10$, $a_2=-0.075$, CN$=3.0$, $\phi=1.0$, $A_B=0.60$.

IV. IPMC ACTUATION

When a cantilevered strip of a fully hydrated IPMC in a metallic cation form is subjected across its faces to, say, 1 V step electric potential, it quickly bends towards the anode. Then, while the voltage is still on, a slow reverse (i.e., towards the cathode) relaxation motion follows the initial fast bending. Upon shorting during the slow bending motion towards the cathode, the IPMC strip quickly bends in the same (i.e., towards the cathode) direction and then reverses its motion and slowly relaxes back towards the anode. In what follows, I seek to model these phenomena micromechanically and obtain quantitative results that are in accord with these observations.

As pointed out before, the application of electric potential causes redistribution of the cations within the membrane. As a result, two thin boundary layers form, one near the anode and the other near the cathode electrodes. In this process, the clusters in the anode boundary layer are depleted of their cations, whereas those in the cathode boundary layer are supplied with additional cations. Recent measurements of the current flow during the IPMC actuation shows continued accumulation of cations within the cathode boundary layer long after the initiation of bending relaxation away from anode and towards the cathode. Thus, during the backrelaxation, the cathode boundary layer of the IPMC strip is contracting while cations are still being added to its clusters. This experimental observation points out the dominance of electrostatic forces over the osmotic and hydraulic pressures (at least during the backrelaxation response), negating the so-called hydraulic model of the IPMC actuation; see Ref. 4.

The anode and cathode boundary layers, together with their corresponding charged electrodes essentially shield the central part of the IPMC from the effects of the applied electric potential. Basically, all critical processes that cause actuation occur within these two boundary layers. Each boundary layer has its own distinct characteristics, which must be understood and modeled.

The cation migration is generally accompanied by some water transport (except for H^+ and for hydrophobic cations, e.g., TMA^+ and TBA^+). In addition, the changes in the ion concentration and in the electrostatic forces that are produced by the cation migration and the resulting charge imbalance within the clusters drive water into or out of the boundary layer clusters. These comments suggest that a complete solution of the actuation problem requires a coupled electrochemomechanical formulation for calculating the charge and water density distributions as functions of time, and thence

the resulting deformation of the IPMC. Suggested by a micromechanical model that did not include the capacitive properties of the electrodes, Nemat-Nasser and Li[24] estimated the time scale for the initial cation redistribution to be very small compared with, say, the mechanical (bending) response time of a hydrated IPMC strip. As mentioned earlier, recent direct measurements[3] have, however, revealed continued cation depletion from the anode and accumulation into the cathode boundary layers long past the initial fast motion and way into the period of backrelaxation of the cantilever. On the other hand, since the widths of the anode and cathode boundary layers (1–20 μm) are small compared with the thickness (about 220 μm) of the hydrated IPMC membrane,[4] the final equilibrium distribution of the cations (under a dc voltage) can be estimated in closed form and then modified to account for the temporal evolution that leads to the final equilibrium state. Therefore, for modeling purposes, one may first calculate the final equilibrium cation distribution that is caused by an applied (dc) electric potential, modify this to include the temporal variation, and then consider the resulting effects on the osmotic, electrostatic, and elastic response of the membrane. The validity of the assumption of the small length of the boundary layers and the separation of spatial and temporal solutions can then be checked *a posteriori*. This approach is followed in the sequel.

A. Volumetric straining, eigenstrain rate, and actuation

I assume that the actuation of the IPMC is caused by the changes in the volume of the clusters within the cathode and anode boundary layers, in response to the electrically induced cation redistribution. In an aqueous environment, I assume full hydration of all the clusters all the time. Thus, when, say, the cation-rich clusters in the cathode boundary layer tend to expand under the action of the repulsive electrostatic forces and osmotic pressure (suction) due to greater cation concentration, I assume that water will diffuse from the surrounding bath into these clusters, keeping the clusters fully saturated. This process continues until the elastic resistance of the matrix polymer in the boundary layers balances the internal cluster pressure. The resulting strains are called eigenstrains. These eigenstrains would result if the boundary layers (clusters embedded in the elastic polymer matrix) were free from the constraint of the remaining part of the IPMC. In the presence of such constraints, elastic stresses are produced in the backbone polymer, leading to the observed bending actuation.

1. Eigenstrain rate

With fully water-saturated clusters, the volumetric strain rate, $\dot{\varepsilon}_\nu$, is related to the rate of change of the water uptake

$$\dot{\varepsilon}_\nu = \frac{\dot{w}}{1+w} = \frac{\partial}{\partial t}\ln(1+w), \tag{31}$$

where, as before, the polymer matrix and water are regarded as incompressible, and hence any overall volume change is due to a change in the cluster volume (water uptake).

With x measuring length along the cross section of the strip (Fig. 7) from its mid-point, denote the corresponding

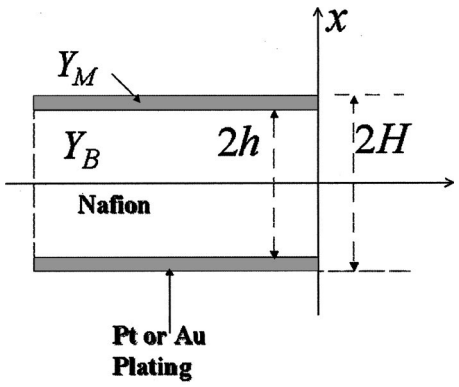

FIG. 7. Schematics of the cross section of an IPMC of thickness $2H$, consisting of metallated layers of thickness H-h sandwiching hydrated bare polymer of thickness $2h$; the effective Young's modulus of the metallated layers is Y_M and that of the hydrated polymer is Y_B; and x measures distance from midpoint of cross section.

axial (along the length of the strip) eigenstrain rate by $\dot{\varepsilon}^*$, and set

$$\dot{\varepsilon}^*(x,t) = \frac{1}{3}\dot{\varepsilon}_\nu(x,t) = \frac{1}{3}\frac{\dot{w}(x,t)}{1+w(x,t)}, \tag{32}$$

where the dependence on the distance along the thickness and time, x and t, is shown explicitly. $\dot{\varepsilon}^*(x,t)$ is called the eigenstrain rate.

2. Eigenstress rate

The eigenstrain rate $\dot{\varepsilon}^*(x,t)$ produces an eigenstress rate,[32] given by

$$\dot{\sigma}^* = -Y_{\mathrm{BL}}\dot{\varepsilon}^*, \tag{33}$$

where Y_{BL} is the effective Young's modulus of the boundary layer, i.e., of the hydrated polymer.

The total axial stress rate acting normal to the cross section of the strip, is given by the sum of the stress rate carried by the backbone polymer, $\dot{\sigma} = \dot{\sigma}(x,t)$, and the eigenstress rate

$$\dot{\sigma}^T(x,t) = \dot{\sigma}(x,t) + \dot{\sigma}^*(x,t). \tag{34}$$

When no external load is applied, equilibrium requires

$$\int_{-\mathrm{H}}^{\mathrm{H}} \dot{\sigma}^T(x,t)\,dx = 0, \quad \int_{-\mathrm{H}}^{\mathrm{H}} x\dot{\sigma}^T(x,t)\,dx = 0. \tag{35}$$

From these expressions, the tip displacement of a cantilevered strip of an IPMC can be computed incrementally, once the eigenstrain rate $\dot{\varepsilon}^*(x,t)$ is known.

Note that the eigenstrains that tend to develop within the boundary layers may be finite. However, the resulting actual bending strains within the IPMC are generally quite small. Therefore, while it may be necessary to use a finite elasticity model to calculate the constraint-free deformation of the clusters in the boundary layers (similar to the stiffness calculation of Sec. III), only small deformation analysis is required for the overall bending calculations.

3. Tip displacement

For a cantilevered strip of length L and unit width, undergoing small bending motion, the tip displacement rate, $\dot{u}$, is related to the maximum cross-sectional bending strain rate $\dot{\varepsilon}_{\max}$ by[33]

$$\dot{\varepsilon}_{\max}=\frac{2H}{L}\frac{\dot{u}}{L}, \tag{36}$$

where $2H$ is the thickness of the hydrated IPMC, and it is assumed that $\dot{\varepsilon}_{\max}$ is constant along the length of the strip. The bending moment required to produce this strain rate is

$$\dot{M}_R=\frac{\dot{\varepsilon}_{\max}}{H}\int_{-\mathrm{H}}^{\mathrm{H}} Y(x)x^2dx\approx\frac{2}{3}\dot{\varepsilon}_{\max}H^2(3\overline{Y}_{\mathrm{IPMC}}-2Y_B), \tag{37}$$

where $\overline{Y}_{\mathrm{IPMC}}$ and $Y_B=3K(w)$ are the Young moduli of the hydrated IPMC and bare Nafion, defined in Eqs. $(30)_1$ and $(21)_1$, respectively. From Eqs. (37) and (36) it now follows that:

$$\frac{\dot{u}}{L}=\frac{3L\dot{M}_R}{4H^3(3\overline{Y}_{\mathrm{IPMC}}-2Y_B)}. \tag{38}$$

Now, using Eqs. (34) in $(35)_2$, the bending moment rate, $\dot{M}_S(x,t)$, supplied by the changes in the boundary layers, is expressed in terms of the rate of water uptake by

$$\dot{M}_S=\frac{1}{3}\int_{-h}^{h} Y_{\mathrm{BL}}x\frac{\dot{w}(x,t)}{1+w(x,t)}dx. \tag{39}$$

If we assume that the boundary layer modulus Y_{BL} is constant, then by setting $\dot{M}_R=\dot{M}_S$, Eq. (38) yields

$$\frac{\dot{u}}{L}=\frac{LY_{\mathrm{BL}}}{4H^3(3\overline{Y}_{\mathrm{IPMC}}-2Y_B)}\int_{-h}^{h} x\frac{\dot{w}(x,t)}{1+w(x,t)}dx. \tag{40}$$

Note that the integration in Eq. (40) is from $-h$ to h, while the total thickness of the strip is $2H$; see Fig. 7.

What remains now is to calculate $\dot{w}(x,t)$ in terms of the osmotic, electrostatic, and elastic forces acting on clusters, as discussed in the sequel.

B. Voltage-induced cation redistribution

In general the redistribution of the cations and the associated water molecules under the action of an applied electric potential, is governed by coupled equations involving the gradient of the chemical potential of water given by Eq. (12), and the electrochemical potential of the cations

$$\mu^+=\mu_0^+ +RT\ln(\gamma^{\pm}\mathrm{C}^+)+F\varphi, \tag{41}$$

as well as the elastic potential of the polymer matrix; in Eq. (41), μ_0^+ includes the reference $\ln(\gamma_0^+C_0^+)$ necessary for normalization, and $\varphi=\varphi(x,t)$ is the electric potential field. The ion and water fluxes must satisfy continuity

$$\frac{\partial}{\partial t}\ln(1+w)+\frac{\partial \nu}{\partial x}=0,\ \frac{\partial \mathrm{C}^+}{\partial t}+\frac{\partial \mathrm{J}^+}{\partial x}=0, \tag{42}$$

where $\nu=\nu(x,t)$ is water velocity (flux) and $\mathrm{J}^+=\mathrm{J}^+(x,t)$ is the cation flux, both in the thickness (i.e., x) direction. These fluxes are usually expressed as linear functions of the gradients $\partial\mu^w/\partial x$ and $\partial\mu^+/\partial x$ (i.e., forces), through empirical coefficients. In a complete theory, these expressions must be appropriately augmented to include the potential of the elastically deforming polymer.

1. Volumetric strain due to cation water transport

As noted before, some water molecules are carried by hydrophilic cations (except for H^+). This kind of water transport must be included directly with the flux of the cation carriers. Indeed, if SN is the dynamic solvation number, i.e., mole water molecules actually transported per mole migrating cations, the resulting volumetric eigenstrain would be

$$\varepsilon_\nu^*=18\times10^{-6}(\mathrm{C}^+-\mathrm{C}^-)\mathrm{SN}. \tag{43}$$

As pointed out in Ref. 4, the interconnected clusters provide an inhomogeneous structure and a tortuous route for the migrating cations. This may result in a solvation number much smaller than what may be measured in the bulk, where water molecules that remain in association with the ion for times longer than the diffusive lifetime are considered solvation waters. Thus, SN in Eq. (43) is expected to be only a fraction of the coordination number, CN, used in the stiffness calculation of Sec. III. This volumetric strain given by Eq. (43) may thus be estimated directly once the cation distribution is calculated and the actual dynamic solvation number for cations in the IPMC is measured (or assumed). I hasten to mention again recent current-flow measurements[3] that show continued cation addition to the cathode clusters while these clusters are actually contacting, suggesting that the cations rather than their solvation water molecules are of primary importance in the IPMC actuation.

2. Cation transport

Consider now the problem of cation redistribution and the associated induced water diffusion. The diffusion-controlled water migration is generally a slow process. Thus, only the second continuity equation in Eq. (42) is expected to be of importance in describing the initial cation redistribution. The corresponding flux can be expressed as

$$\mathrm{J}^+=-\frac{\mathrm{D}^{++}\mathrm{C}^+}{RT}\frac{\partial\mu^+}{\partial x}+\frac{\mathrm{D}^{+w}\mathrm{C}^+}{RT}\frac{\partial\mu^w}{\partial x}, \tag{44}$$

where D^{++} and D^{+w} are empirical coefficients. From Eqs. (41) and (44), it follows that:

$$\mathrm{J}^+=-\mathrm{D}^{++}\left(\frac{\partial \mathrm{C}^+}{\partial x}+\frac{\mathrm{C}^+F}{RT}\frac{\partial\varphi}{\partial x}\right)+\frac{\mathrm{D}^{+w}\mathrm{C}^+}{RT}\frac{\partial\mu^w}{\partial x}. \tag{45}$$

On the other hand, the well-known Nernst equation yields, in the present case[34]

$$\mathrm{J}^+=-\mathrm{D}^+\left(\frac{\partial \mathrm{C}^+}{\partial x}+\frac{\mathrm{C}^+F}{RT}\frac{\partial\varphi}{\partial x}+\frac{\mathrm{C}^+\mathrm{V}^{+w}}{RT}\frac{\partial p}{\partial x}\right)+\mathrm{C}^+\nu, \tag{46}$$

with D^+ being the ionic diffusivity coefficient. Since only the first two terms in the parentheses contribute to the final linearized equation governing the cation redistribution,[24,4] the two approaches lead to the same results under the stated assumptions in the present case.

The variation of the electric potential field, $\varphi=\varphi(x,t)$, in the membrane is governed by the basic electrostatics equations

$$\frac{\partial D}{\partial x}=(\mathrm{C}^+-\mathrm{C}^-)F, \quad D=\kappa E, \quad E=-\frac{\partial \varphi}{\partial x}, \tag{47}$$

where D, E, and κ are the electric displacement, electric field, and the electric permittivity, respectively. These are all functions of both x and t. Combining Eqs. (46) to (47) and neglecting small terms,[24,4] we obtain

$$\frac{\partial}{\partial x}\left\{\frac{\partial(\kappa E)}{\partial t}-D^+\left[\frac{\partial^2(\kappa E)}{\partial x^2}-\frac{\mathrm{C}^-F^2}{\kappa RT}(\kappa E)\right]\right\}=0. \tag{48}$$

This equation provides a natural length scale, ℓ, and a natural time scale, τ, which characterize the length of the boundary layers and the relative speed of cation redistribution. These are

$$\ell=\left(\frac{\overline{\kappa}RT}{\mathrm{C}^-F^2}\right)^{1/2}, \quad \tau=\frac{\ell^2}{\mathrm{D}^+}, \tag{49}$$

where $\overline{\kappa}$ is the overall electric permittivity of the hydrated IPMC strip, which can be estimated from its measured capacitance.[35] Therefore, ℓ can be estimated directly from Eq. $(49)_1$, whereas the estimate of τ will require an estimate for D^+. It turns out that the capacitance of the Nafion-based IPMCs (about 200–225 μm thick) that have been examined in my laboratories, ranges from 1 to 60 mF/cm^2, depending on the sample and the cation form. This suggests that ℓ may be 0.5–6 μm, for the Nafion-based IPMCs. Thus, ℓ^2 is of the order of 10^{-12} m^2, and for the relaxation time τ to be of the order of seconds, D^+ must be of the order of 10^{-12} m^2/s. Our most recent experimental results[3] suggest this to be the case. Indeed, direct measurement of current flow through Nafion-based IPMC strips under a constant voltage shows $\tau=O(1)s$ in an aqueous environment.

Since ℓ is linear in $\sqrt{\overline{\kappa}}$ and $\overline{\kappa}$ is proportional to the capacitance, it follows that ℓ is proportional to the square root of the capacitance.

3. Equilibrium ion distribution

To calculate the ion redistribution caused by the application of a step voltage across the faces of a hydrated strip of IPMC, we first examine the time-independent equilibrium case with $\mathrm{J}^+=0$. Here we seek to include the asymmetry in the cation distribution that has been neglected in the calculation of Ref. 24, arriving at more realistic estimates.[36] To this end, we note that in the cation-depleted (anode) boundary layer the charge density is constant, given by $-\mathrm{C}^-F$, whereas in the remaining part of the membrane the charge density is given by $(\mathrm{C}^+-\mathrm{C}^-)F$. Let the thickness of the cation-depleted zone with constant charge density of $-\mathrm{C}^-F$ be denoted by ℓ'. The electric field in the zone $-h\leqslant\overline{x}\leqslant -h+\ell'$, is then given by

$$\kappa(x)E^{(1)}(x)=-\mathrm{C}^-Fx+\overline{E}_0, \tag{50}$$

where $\overline{E}_0$ is an integration constant. To simplify the analysis, we replace $\kappa=\kappa(x)$ by its constant effective value $\overline{\kappa}$, and from Eqs. (50) and $(47)_3$ obtain

$$E^{(1)}(x)=\frac{1}{\ell}\left(-K_0\frac{x}{\ell}+E_0\right), \quad K_0=\frac{\mathrm{C}^-F\ell^2}{\overline{\kappa}}=\frac{RT}{F},$$
$$\varphi^{(1)}(x)=K_0\left(\frac{x}{\ell}\right)^2-E_0\frac{x}{\ell}+A_0, \tag{51}$$

where E_0 and A_0, as well as ℓ' are constants to be computed from the boundary and continuity conditions, discussed in the sequel. Solution (51) is considered to hold in the region $-h\leqslant x\leqslant -h+\ell'$. In the remaining region along the thickness, i.e., in $-h+\ell'<x\leqslant h$, we integrate the basic equation

$$\frac{\partial^2 E}{\partial x^2}-\frac{1}{\ell^2}E=0, \tag{52}$$

to arrive at

$$E^{(2)}(x)=\frac{1}{\ell}[B_0\exp(x/\ell)+B_1\exp(-x/\ell)],$$
$$\varphi^{(2)}(x)=-B_0\exp(x/\ell)+B_1\exp(-x/\ell)+B_2, \tag{53}$$
$$\frac{\mathrm{C}^+(x)-\mathrm{C}^-}{\mathrm{C}^-}=\frac{F}{RT}[B_0\exp(x/\ell)-B_1\exp(-x/\ell)],$$

where B_0, B_1, and B_2 are the integration constants. These and the other constants are calculated from the following continuity, boundary, and the overall charge-balance conditions

$$\begin{aligned}
&\mathrm{C}^+(-h')=0, \quad h'=h-\ell',\\
&E^{(1)}(-h')=E^{(2)}(-h'),\\
&\varphi^{(1)}(-h')=\varphi^{(2)}(-h'),\\
&\varphi^{(1)}(-h)=\phi_0/2,\\
&\varphi^{(2)}(h)=-\phi_0/2,\\
&\int_{-h}^{h}(\mathrm{C}^+-\mathrm{C}^-)dx=0.
\end{aligned} \tag{54}$$

Since ℓ is only 0.5–3 μm, the resulting system of equations can be solved explicitly by noting that $(a\equiv h/\ell,\ a'\equiv h'/\ell)\gg 1$, and hence, $\exp(-a)\approx 0$ and $\exp(-a')\approx 0$. The final results are

$$\begin{aligned}
&E_0=K_0(1-a'), \quad A_0=\frac{\phi_0}{2}-K_0\left(1+\frac{\ell'}{\ell}-2a\right),\\
&B_1=K_0\exp(-a'), \quad \frac{\ell'}{\ell}=\sqrt{\frac{2\phi_0F}{RT}}-2,\\
&B_2=\frac{\phi_0}{2}-\frac{1}{2}K_0\left[\left(\frac{\ell'}{\ell}+1\right)^2+1\right],\\
&B_0=\exp(-a)[\phi_0/2+B_1\exp(-a)+B_2].
\end{aligned} \tag{55}$$

Constants A_0, E_0, and B_2 are finite, being of the order of 10, 1, and 0.1, respectively. On the other hand, constants B_0 and B_1 are very small, being of the order of 10^{-17} or even smaller, depending on the value of the capacitance. Therefore, the approximation used to arrive at Eq. (55) does not compromise the accuracy of the results. Numerical evaluation supports this conclusion.

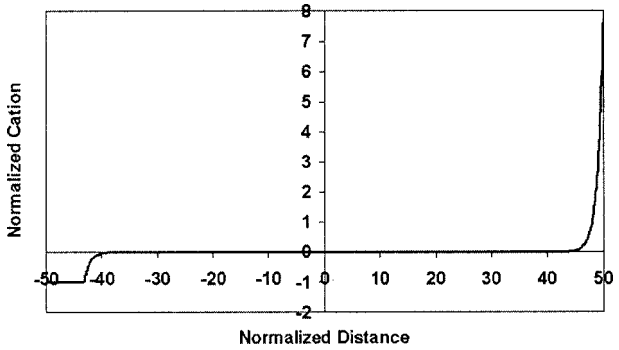

FIG. 8. Variation of the normalized charge density, $(C^+-C^-)/C^-$, through the thickness of an IPMC with $a=50$ and $\phi_0=1$ V.

4. Length of boundary layers

Remarkably, the estimated length of the anode boundary layer with constant negative charge density of $-C^-F$, i.e., $\ell'=(\sqrt{2\phi_0 F/RT}-2)\ell$, depends only on the applied potential and the characteristic length ℓ. For $\phi_0=1$ V, for example, $\ell'\approx 6.8\ell$. Since ℓ is proportional to the square root of $\overline{\kappa}$, and $\overline{\kappa}$ is proportional to the IPMC's capacitance, it follows that ℓ' varies as the square root of the capacitance. It will be shown below that the tip displacement of a cantilevered strip of an IPMC is a monotonically increasing function of ℓ and, hence, varies (increases linearly) monotonically with the square root of the capacitance. This fact underpins the significance of developing optimal electrode morphology to maximize the resulting capacitance in order to achieve greater actuation.

We use ℓ as our length scale. Then, for a fixed value of the magnitude of an applied step potential, ϕ_0, we observe from Eqs. (51), (53), and (55) that the equilibrium distribution of the resulting internal potential and the cations, depends on $a=h/\ell$ only. Figure 8 illustrates the final equilibrium variation of the normalized charge density, $(C^+-C^-)/C^-$, through the thickness of an IPMC with $a=50$ and $\phi_0=1$ V. As is seen, over the most central part of the membrane, there is charge neutrality within all clusters, and the charge imbalance in clusters occurs only over narrow boundary layers, with the anode boundary layer being thicker than the cathode boundary layer. It should be emphasized that equilibrium requires electric neutrality everywhere in the IPMC strip, even within its electrode regions, and that the charge imbalance in the clusters is actually balanced by the corresponding electrode charges. Therefore, the charge imbalance calculated earlier applies to the clusters within each boundary layer and not to the boundary layer itself, i.e., not to the combined clusters and the charged metal particles within the boundary layers.

5. Temporal variation of charge distribution

We now examine the time variation of the charge distribution that results upon the application of a step voltage and leads to the equilibrium solution given above. To this end, consider Eq. (48), and rewrite it as

$$\frac{\partial}{\partial x}\left\{\frac{\partial(\kappa E)}{\partial t}-D^+\left[\frac{\partial^2(\kappa E)}{\partial x^2}-\frac{1}{\ell^2}(\kappa E)\right]\right\}=0, \tag{56}$$

where only in the expression for ℓ^2 have we approximated the variable electric permittivity, κ by its average effective value, $\overline{\kappa}$. In view of Eq. (47) and if C^- is assumed to remain constant[37] then Eq. (56) becomes

$$\frac{\partial Q}{\partial t}-D^+\left(\frac{\partial^2 Q}{\partial x^2}-\frac{Q}{\ell^2}\right)=0,\quad Q=\frac{C^+-C^-}{C^-}\geqslant -1. \tag{57}$$

Now set $Q_0(x)=\lim_{t\to\infty} Q(x,t)$ and note that

$$Q_0(x)\equiv\begin{cases} -1 \quad \ldots \text{for } x\leqslant -h+\ell' \\ \dfrac{F}{RT}[B_0\exp(x/\ell)-B\exp(-x/\ell)]. \\ \qquad \ldots \text{for} -h+\ell'<x<h \end{cases} \tag{58}$$

Then, the solution of Eq. (57) can be expressed by $Q=\psi(x,t)\exp(-t/\tau)+Q_0(x)$, where $\psi(x,t)$ is now defined by the following diffusion equation and initial condition:

$$\frac{\partial\psi}{\partial t}=D^+\frac{\partial^2\psi}{\partial x^2},\quad \psi(x,0)=-Q_0(x), \tag{59}$$

subject to zero cation flux in and out of the membrane at its boundary surfaces, i.e., $J^+(\pm h,t)=0$. The solution can be expressed in Fourier series by

$$\begin{aligned} &\psi=\sum_{n=1}^{\infty}[a_n\cos(z_n x/h)+b_n\sin(z_n x/h)] \\ &\qquad\times\exp\{-z_n^2 t/(a^2\tau)\}, \\ &\sum_{n=1}^{\infty}[a_n\cos(z_n x/h)+b_n\sin(z_n x/h)]=Q_0(x), \end{aligned} \tag{60}$$

where z_n, $n=1,2,3,...$, is of the order of n, and the Fourier coefficients are obtained from Eq. $(60)_2$ in the usual manner. Since these coefficients quickly diminish with increasing n, and since $a=h/\ell\approx 50$, we conclude that

$$Q(x,t)\approx g(t)Q_0(x),\quad g(t)=1-\exp(-t/\tau). \tag{61}$$

Thus, the spatial variation of the charge distribution can be separately analyzed and then modified to include the temporal effects.

C. Fast actuation, slow reverse relaxation

With the cation distribution given by Eqs. (58) and (61), the pressure within the clusters of each boundary layer is now computed, and from this the resulting volumetric changes within the boundary layers are obtained, as follows.

1. Anode boundary layer

Consider first the anode boundary layer, and note from

$$\int_{-h'}^{0} Q_0(x)\,dx=\ell \tag{62}$$

that the effective total length of the anode boundary layer, L_A, can be taken as

$$L_A\equiv\ell'+\ell=\left(\sqrt{\frac{2\phi_0 F}{RT}}-1\right)\ell. \tag{63}$$

To simplify calculation, consider a constant equilibrium charge density of $Q_0(x)=-1$, in $-h\leqslant x<-h+L_A$, and zero for the remaining zone, $-h+L_A\leqslant x<0$. Hence, identify the anode boundary layer by the zone $-h\leqslant x<-h+L_A$ and obtain $C^+=C^-\exp(-t/\tau)$ in this layer. The total ion (cation and anion) concentration within this layer now is given by $C^-+C^+=C^-[2-g(t)]$. Thus, the osmotic pressure in the clusters within the anode boundary layer is given by Eq. (13) with $\nu=1+\exp(-t/\tau)=2-g(t)$,

$$\Pi_A(t)=\frac{\phi Q_B^- K_0}{w_A(t)}[2-g(t)], \tag{64}$$

where Q_B^- and K_0 are defined in Eqs. (15) and (17), respectively.

As the cations of the anode boundary layer are depleted, electrostatic interaction forces develop among the fixed anions, introducing additional pressure, say, p_{AA}, within the cluster, while at the same time, the dipole–dipole interaction forces, p_{ADD}, are being diminished. The two effects are coupled, since the cation distribution within a cluster would depend on its concentration. We simplify the required analysis and assume the two effects are uncoupled.

To calculate p_{AA} as a function of time, consider an elementary surface of a spherical cluster with uniformly distributed surface charge q given by Eq. (15), calculate the Coulomb interaction forces, and then multiply the result by $g(t)$, to obtain,

$$\begin{aligned} p_{AA}(t)&=\frac{q^2 g(t)}{2\kappa_A(t)}=\frac{g(t)}{18\kappa_A(t)}Q_B^{-2}\frac{a_A^2}{[w_A(t)]^2}\\ &\approx\frac{g(t)}{18\kappa_A(t)}Q_B^{-2}\frac{R_0^2}{[w_A(t)]^{4/3}}, \end{aligned} \tag{65}$$

where $\kappa_A=\kappa_A(t)$ is the effective electric permittivity of the cluster, a_A is the radius of the cluster at water uptake $w_A=w_A(t)$, R_0 is the initial (dry) cluster size, and the subscript A refers to the anode boundary layer; all other parameters are as defined before. The corresponding p_{ADD} (the subscript A denotes the anode boundary layer) is estimated from Eq. (16) using the cation concentration in each cluster

$$p_{\mathrm{ADD}}(t)=\frac{1-g(t)}{3\kappa_A(t)}Q_B^{-2}\frac{\pm[\alpha_A(t)]^2}{[w_A(t)]^2}. \tag{66}$$

The total pressure within a typical cluster in the anode boundary layer, hence, is

$$p_A=\Pi_A(M^+,t)+p_{AA}(t)+p_{\mathrm{ADD}}(t). \tag{67}$$

Based on the ion concentration in clusters within the anode boundary layer, the effective electric permittivity κ_A becomes, for $m_{wA}-\mathrm{CN}\geqslant 0$:

$$\begin{aligned} &\kappa_A=\frac{7+6f_A}{7-6f_A}6\kappa_0,\quad f_A=\frac{m_{wA}-\mathrm{CN}}{m_{wA}},\\ &m_{wA}(t)=\frac{\mathrm{EW}_{\mathrm{ion}}w_A(t)}{18[2-g(t)]\rho_B}, \end{aligned} \tag{68}$$

where $m_{wA}(t)$ is the total mole water per mole ion, and $f_A(t)$ is the fraction of free water molecules within a cluster in the anode boundary layer. If $m_{wA}-\mathrm{CN}<0$, then we set $\kappa_A=6\kappa_0$.

Pressure $p_A(t)$ is resisted by the elastic stress, $\sigma_r(a_0,t)=-p_0(t)+K(t)[w_A(t)/w_0]^{-4/3}$, in the matrix polymer, and balance is attained once equilibrium is achieved. This resistive stress is given by Eq. $(10)_1$, where for the stiffness $K(t)$ and pressure $p_0(t)$, we use expressions (21) associated with the bare polymer at the corresponding hydration, w_A. The resulting effective pressure acting on the water within the anode boundary layer is thus given by

$$t_A(t)=-\sigma_r(a_0,t)+p_A(t). \tag{69}$$

This stress is not zero during the cation redistribution. The result is water diffusion into or out of the anode boundary layer depending on whether $t_A(t)$ is less than or greater than the effective pressure p_R of the surrounding bath water. The water exchange can be computed using the diffusion equation and the initial and boundary conditions. However, since the boundary layer is rather thin, we may simplify the necessary calculations by assuming uniform w_A and t_A in the boundary layer. Then the differential Eq. $(42)_1$ can be replaced by the following difference equation:

$$\frac{\dot{w}_A}{1+w_A}+\frac{\nu_A-\nu_R}{(L_A/2)}=0, \tag{70}$$

where the velocity $\nu_R=0$ when the IPMC strip is actuated while submerged in a large bath of pure water, and the velocity ν_A can be assumed to be linearly related to the differential pressure

$$\nu_A=D_{\mathrm{H_2O}}\frac{t_A-p_R}{(L_A/2)}, \tag{71}$$

where $D_{\mathrm{H_2O}}$ is the hydraulic permeability coefficient. With this approximation, and setting the reference pressure p_R equal to zero, we obtain

$$\frac{\dot{w}_A}{1+w_A}=D_{\mathrm{H_2O}}\frac{t_A}{(L_A/2)^2}=D_A t_A. \tag{72}$$

Note that coefficient D_A here includes the effect of the thickness of the boundary layer. We assume that D_A is constant.

2. Cathode boundary layer

Consider now the clusters within the cathode boundary layer. Unlike the anode boundary layer, the ion concentration in the cathode boundary layer is sharply variable and, in view of Eq. $(53)_3$, it may be expressed by the parameter

$$\nu_C(x,t)=2+Q(x,t)=2+\frac{B_0}{K_0}\exp(x/\ell)g(t). \tag{73}$$

The osmotic pressure in the clusters within the cathode boundary layer is now obtained by setting $\nu=\nu_C(x,t)$ in expression (13), arriving at

$$\Pi_C(x,t)=\frac{\nu_C(x,t)\phi Q_B^- K_0}{w_C(x,t)}, \tag{74}$$

where $w_C(x,t)$ is the volume fraction of water in the cathode boundary layer, depending on both x and t.

In the cathode boundary layer there are two forms of electrostatic interaction forces. One is repulsion due to the cation-anion pseudo-dipoles already present in the clusters, and the other is due to the extra cations that migrate into the clusters and interact with the existing pseudo-dipoles. The additional stresses produced by this latter effect may tend to expand or contract the clusters, depending on the distribution of cations relative to the fixed anions. We again model each effect separately, although in actuality they are coupled. The dipole–dipole interaction pressure in the clusters is estimated using Eq. (16), as follows:

$$p_{C\mathrm{DD}}(x,t)=\frac{Q_B^{-2}}{3\kappa_C(x,t)}\frac{\pm[\alpha_C(x,t)]^2}{[w_C(x,t)]^2}[1-g(t)], \tag{75}$$

where the subscript C denotes the corresponding quantity in the cathode boundary layer; $\alpha_C(x,t)$ is the dipole arm that can evolve in time, as the cations reconfigure under the action of the strong sulfonates (but not necessarily under the action of the weak carboxylates). We represent the interaction between the pre-existing dipoles and the additional cations that move into a cluster under the action of an applied voltage, by dipole-cation interaction stresses defined by

$$p_{\mathrm{DC}}(x,t)=\frac{2Q_B^{-2}}{9\kappa_C(x,t)}\frac{a_C(x,t)\alpha_C(x,t)}{[w_C(x,t)]^2}g(t)$$
$$\approx\frac{2Q_B^{-2}}{9\kappa_C(x,t)}\frac{R_0\alpha_C(x,t)}{[w_C(x,t)]^{5/3}}g(t). \tag{76}$$

This equation is obtained by placing the extra cations at the center of a sphere of (current) radius $a_C(x,t)$, which contains uniformly distributed radial dipoles of moment arm $\alpha_C(x,t)$ on its surface, and then multiplying the result by $g(t)=1-\exp(-t/\tau)$.

For sulfonates in a Nafion-based IPMC, we expect extensive restructuring and redistribution of the extra cations. It appears that this process underpins the observed reverse relaxation of the Nafion-based IPMC strip. Indeed, this redistribution of the cations within the clusters in the cathode boundary layer may quickly diminish the value of p_{DC} to zero or even render it negative. To represent this, we modify Eq. (76) by a relaxation factor, and write

$$p_{\mathrm{DC}}(x,t)\approx\frac{2Q_B^{-2}}{9\kappa_C(x,t)}\frac{R_0\alpha_C(x,t)}{[w_C(x,t)]^{5/3}}g(t)g_1(t),$$
$$g_1(t)=[r_0+(1-r_0)\exp(-t/\tau_1)],\quad r_0<1, \tag{77}$$

where τ_1 is the relaxation time, and r_0 is the equilibrium fraction of the dipole-cation interaction forces.

The total stress in clusters within the cathode boundary layer is now approximated by

$$t_C=-\sigma_r(a_0,t)+\Pi_C(x,t)+p_{C\mathrm{DD}}(x,t)+p_{\mathrm{DC}}(x,t). \tag{78}$$

Expression (58) and Fig. 8 reveal an exponential variation of cation distribution in a very thin cathode layer. We use a linear diffusion model to relate the water flux (diffusion water velocity), ν_C, to the driving pressure gradient $\partial t_C/\partial x$:

$$\nu_C=-D_{\mathrm{H_2O}}\frac{\partial t_C}{\partial x}. \tag{79}$$

Hence, in view of the continuity condition $(42)_1$, the rate of change of water uptake in the cathode boundary layer is governed by the diffusion equation

$$\frac{\dot{w}_C}{1+w_C}=D_{\mathrm{H_2O}}\frac{\partial^2 t_C}{\partial x^2}, \tag{80}$$

subject to the boundary and initial conditions

$$t_C(h,t)=p_R=0,\ \ w_C(0,t)=w_0,\ \ t>0,$$
$$w_C(x,0)=w_0\ \ 0<x<h, \tag{81}$$

where w_0 is the uniform water uptake just prior to the cation redistribution.

Even with the linear flux-force relation, this is a highly nonlinear initial-boundary value problem, since the dependence of the driving force, $t_C(x,t)$, on w_C is nonlinear and complex. Thus, a complete solution would require a numerical approach. Since our basic aim is to reveal the essential micromechanisms of the actuation, we take advantage of the thinness of the cathode boundary layer to simplify this problem. Therefore, we again replace the spatial gradients by the corresponding difference expression, and solve for an average value of the water uptake in the boundary layer.

Because of the overall charge neutrality, the total added cations in the cathode boundary layer satisfies

$$\int_0^h Q(x,t)dx=L_A g(t). \tag{82}$$

Let L_C denote the effective length of an equivalent cathode boundary layer with uniform cation distribution, calculate this length by locating the centroid of the cation distribution from the origin, and then set

$$L_C=2\left[h-\frac{1}{L_A}\int_0^h xQ_0(x)dx\right]. \tag{83}$$

The average ion density (mol/m^3 of hydrated membrane) in this layer is given by

$$\overline{\nu}_C C^-=\left[2+\frac{L_A}{L_C}g(t)\right]C^-. \tag{84}$$

To calculate the osmotic pressure term in Eq. (78), we use the average value

$$\overline{\nu}_C(t)=2+\frac{L_A}{L_C}g(t). \tag{85}$$

For this equivalent cathode boundary layer with uniform ion and water distribution, we now follow the same argument that led to Eq. (72), use the average (spatially constant) values of ion concentration $\overline{\nu}_C(t)$, given by Eq. (85), and water $\overline{w}_C(t)$, in Eqs. (74)–(78), and obtain

$$\frac{\dot{w}_C}{1+w_C}=D_C\overline{t}_C, \tag{86}$$

where

$$\overline{t}_C(t)=-\overline{\sigma}_r(a_0,t)+\overline{\Pi}_C(t)+\overline{p}_{C\mathrm{DD}}(t)+\overline{p}_{\mathrm{DC}}(t), \tag{87}$$

where the barred quantities denote the average values. Since the thickness of the anode and that of the equivalent cathode boundary layer is not the same, we expect

$$D_C=\left(\frac{L_A}{L_C}\right)^2 D_A. \tag{88}$$

3. Tip displacement

The tip displacement of the cantilever may now be calculated incrementally, using Eq. (40). For the equivalent uniform boundary layers, the integral in the right-hand side of this equation can be computed in closed form, yielding

$$\frac{\dot{u}}{L}=\frac{Y_{\mathrm{BL}}}{(3\overline{Y}_{\mathrm{IPMC}}-2Y_B)}\frac{hL}{4H^2}\left(\frac{\dot{w}_A}{1+w_A}\frac{L_A}{H}-\frac{\dot{w}_C}{1+w_C}\frac{L_C}{H}\right), \tag{89}$$

where we have neglected terms of the order of $O(L_A/H)^2$. Combining this with Eqs. (72), (85), and (88), we now have

$$\frac{\dot{u}}{L}=\frac{Y_{\mathrm{BL}}}{(3\overline{Y}_{\mathrm{IPMC}}-2Y_B)}\frac{hLL_A}{4H^3}D_A\left(t_A-\overline{t}_C\frac{L_A}{L_C}\right), \tag{90}$$

where t_A and $\overline{t}_C$ are given by Eqs. (69) and (87), respectively. This equation may now be integrated incrementally.

D. Response upon shorting

When an applied constant potential is maintained on the cantilevered strip, the strip relaxes into a final equilibrium state. If during this relaxation phase, the two faces of the strip are suddenly shorted, some cations move into the cation-depleted clusters of the anode boundary layer, while some (but not necessarily all) of the extra cations in the clusters of the cathode boundary layer move into the interior of the polymer. Over time, a uniform cation distribution may eventually be attained, but in the short run the discharge is seldom complete. With the initial condition known at the instant of shorting, say, at $t=T_s$, and using the same relaxation time of τ for the discharge, we set

$$Q(x,t)=Q_0(x)[g(t)-(1-r)g(t-T_s)], \tag{91}$$

for $t\geqslant T_s$, where r is the fraction of ions that do not discharge in the short run. Based on this, the cluster pressure can be estimated. We examine the anode and cathode boundary layers, separately, as follows.

In the anode boundary layer, we have, for $t\geqslant T_s$:

$$\Pi_A(t)=\frac{\phi Q_B^- K_0}{w_A(t)}[2-g(t)+(1-r)g(t-T_s)], \tag{92}$$

$$p_{AA}(t)\approx\frac{Q_B^{-2}R_0^2}{18\kappa_A(t)[w_A(t)]^{4/3}}[g(t)-(1-r)g(t-T_s)], \tag{93}$$

$$p_{\mathrm{ADD}}(t)=\frac{\pm[\alpha_A(t)]^2Q_B^{-2}}{3\kappa_A(t)[w_A(t)]^2}[1-g(t)+(1-r)g(t-T_s)]. \tag{94}$$

In addition, Eq. $(68)_3$ is modified to read

$$m_{wA}(t)=\frac{\mathrm{EW}_{\mathrm{ion}}w_A(t)}{18[2-g(t)+(1-r)g(t-T_s)]\rho_B}. \tag{95}$$

These equations are obtained by simply assuming that the discharge is the reverse of the charging process, although in reality the various involved processes are coupled.

In the cathode boundary layer, we have, for $t\geqslant T_s$:

$$\overline{\Pi}_C(t)=\frac{\phi Q_B^- K_0}{w_A(t)}\left\{2+\frac{L_A}{L_C}[g(t)-(1-r)g(t-T_s)]\right\}, \tag{96}$$

$$\overline{p}_{\mathrm{CDD}}(t)\approx\frac{\pm[\alpha_A(t)]^2Q_B^{-2}}{3\overline{\kappa}_C(t)[\overline{w}_C(t)]^2}[1-g(t)+(1-r)g(t-T_s)], \tag{97}$$

$$\overline{p}_{\mathrm{DC}}(t)\approx\frac{2Q_B^{-2}}{9\overline{\kappa}_C(t)}\frac{R_0\overline{\alpha}_C(t)}{[\overline{w}_C(t)]^{5/3}}[1-g(t-T_s)]g_1(t). \tag{98}$$

In addition, we use

$$m_{wC}(t)=\frac{\mathrm{EW}_{\mathrm{ion}}\overline{w}_C(t)}{18\{2+(L_A/L_C)[g(t)-(1-r)g(t-T_s)]\}\rho_B} \tag{99}$$

to estimate mole water per mole ion in the cathode boundary layer.

E. Illustrative example

To illustrate how the model may capture the essential features of actuation of IPMCs, we now consider a cantilevered strip of the Nafion-based IPMC in the Li^+ form, for which we have examined the Young's modulus as a function of the hydration in Fig. 5. We apply 1 V potential across its faces, maintain this for 31 s, and then short the two faces. We seek to predict the resulting actuation, based on the proposed model.

1. Initial data

The gauge length of the strip is about 18 mm, and its initial hydration is $w_{\mathrm{IPMC}}=0.50$. Hence, the initial volume fraction of water in the Nafion part of the IPMC is calculated, yielding $w_0=w_{\mathrm{IPMC}}/(1-f_M)=0.533$. From Eq. (1) the equivalent weight for the bare Nafion (and not the IPMC) is obtained to be $\mathrm{EW}_{\mathrm{Li}^+}=1106$ g/mol. The initial value of C^- for the bare Nafion is then given by

$$C^-=10^6\frac{\rho_B}{\mathrm{EW}_{\mathrm{Li}^+}(1+w_0)}=1185\ \mathrm{mol/m^3}.$$

The thickness of the hydrated strip is measured to be $2H=224\ \mu$m, and based on inspection of the microstructure of the electrodes (Fig. 2), we estimate $2h\approx212\ \mu$m. The effective length of the anode boundary layer is given by Eq. (63). For $\phi_0=1$ V, we have $L_A=7.80\ell$. The thickness of the equivalent uniform cathode boundary layer is calculated from Eq. (83), obtaining $L_C=3.58\ell$. The electric permittivity and the dipole length are the same as before, with the same values of the parameters that have been obtained in the modeling of the Young's modulus. The measured capacitance ranges from 1 to 30 mF/cm^2.

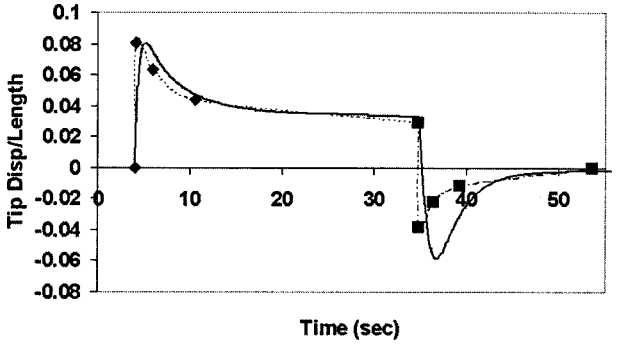

FIG. 9. Tip displacement of a 18 mm cantilevered strip of a Nafion-based IPMC in Li^+ form, subjected to 1 V step potential for about 31 s, then shorted; the heavy solid curve is model and the geometric symbols connected by light dotted curve are experimental points.

2. Model parameters

The model parameters that must now be estimated are D_A, R_0, τ, and SN, as well as r_0 and τ_1 in the relaxation function $g_1(t)$. We set SN$=0$. This is in line with the observation that the cations continue to move into the cathode boundary layer long after the backrelaxation has started.

It turns out that R_0 must be calculated with some care. Since $w_0 \approx (a/R_0)^3$, where a is the cluster size at water uptake w_0, we set $R_0 \approx w_0^{-1/3} a$, and adjust a to fit the experimental data; here, we set $a=1.60$ nm, or an average cluster size of 3.2 nm, prior to the application of the potential. The two relaxation times are set at $\tau = 1/4s$ and $\tau_1 = 4s$, respectively, and $r_0 = 0.6$.

We set $D_A = 1.0\times 10^{-2}$ when pressure is measured in mega pascal. This is somewhat arbitrary and is chosen to yield reasonable results. Larger values of this parameter produce sharper rise and decay in the tip displacement. Finally we choose a low value for the capacitance, namely 1.2 mF/cm^2, since this value seems to give results in accord with the experimental data, as shown in Fig. 9. With this value for the capacitance, the overall effective electric permittivity of the hydrated IPMC becomes, $\overline{\kappa} = 2.69\times 10^{-3}$ F/m. Then Eq. $(49)_1$ gives, $\ell = 0.779\ \mu$m.

It is important to note that while the values of the parameters that are used are reasonable, they have been chosen to give good comparison with specific experimental data. These data are from one test only. The variation of the response from sample to sample (or even for the same sample tested at various times) is often so great that only a qualitative correspondence between the theoretical predictions and the experimental result can in general be expected, or reasonably required. In examining the influence of various competing factors, it has become clear that the electrostatic forces are most dominant, as has also been observed by Nemat-Nasser and Li[24] using a different approach. Although the osmotic effects are also relevant, they have less impact in defining the initial actuation and subsequent relaxation of the Nafion-based IPMCs. The formulation presented in this article gives detailed structure to each competing factor, and suggests a path for further parametric and experimental studies.

V. CONCLUSIONS

- For a given ionomer (Nafion or Flemion), the morphology of the electrodes and the nature of the neutralizing cations are the most important parameters affecting the actuation of a fully hydrated IPMC.
- To maximize the tip displacement of a cantilevered strip with its bending stiffness held fixed, it is necessary to maximize the capacitance and surface conductivity of the IPMC.
- Once an electric potential is applied across the faces of the cantilever, two thin boundary layers form near the surface within the IPMC, one near the anode and the other near the cathode. Recent direct measurements[3] have revealed continued cation depletion from the anode and accumulation into the cathode boundary layers long past the initial fast motion and way into the period of backrelaxation of the cantilever that is actuated by a dc voltage. At equilibrium, the anode boundary layer is depleted of its cations while the cathode boundary layer is rich with additional cations.
- The effective length of the anode boundary layer is given by
$$L_A = \left(\sqrt{\frac{2\phi_0 F}{RT}} - 1 \right) \ell, \quad \ell = \sqrt{\frac{2H\mathrm{Cap}RT}{\mathrm{C}^- F^2}},$$
where ϕ_0 is the applied potential and Cap is the capacitance.
- The extra cations within the cathode boundary layer are given by
$$\int_0^h (\mathrm{C}^+ - \mathrm{C}^-)\, dx = L_A \mathrm{C}^-,$$
which is proportional to ℓ.
- The internal forces created within the anode and cathode boundary layers by the resulting ion redistribution, increase with increasing L_A and, hence, with increasing $\sqrt{\mathrm{Cap}}$.
- For a fully hydrated IPMC membrane, the equilibrium distribution of the cations and the internal potential that develops under the action of an applied step potential of magnitude ϕ_0, depend on $a = h/\ell$ and ϕ_0 only.
- The model must be modified for application to IPMCs that are neutralized by large hydrophobic organic cations such as TBA.
- The variation of the response from sample to sample (or even for the same sample tested at various times) is often so great that only a qualitative correspondence between the theoretical predictions and the experimental result can in general be expected, or reasonably required.

I hope that the micromechanical model presented in this work would provide a tool to identify important parameters that can be used to optimize the response of IPMCs through improved processing techniques.

ACKNOWLEDGMENTS

The author wishes to thank Dr. Steve Wax (DARPA), Dr. Len Buckley (NRL), Dr. Carlos Sanday (NRL), and Dr. Randy Sands for their continued encouragement and many stimulating discussions. The author thanks Professor Mohsen Shahinpoor and Dr. K. J. Kim for providing IPMC materials

and many informative discussions; Dr. Yosi Bar-Cohen for his continued interest and stimulating interaction; colleagues Professors Yitzhak Tor and Mike Sailor for comments and discussions; co-workers Jon Isaacs and David Lischer for their assistance; Dr. Chris Thomas [who also created Fig. 2(a)] and graduate student Jeff McGee for helpful discussions; and graduate student Sai Sarva who produced data for Fig. 3. This work has been supported by DARPA Grant No. MDA972-00-1-0004 to the University of California, San Diego.

[1] K. Asaka and K. Oguro, J. Electroanal. Chem. **480**, 186 (2000).
[2] Y. Bar-Cohen, S. P. Leary, M. Shahinpoor, J. S. Harrison, and J. Smith, Proc. SPIE **3669**, 51 (1999).
[3] S. Nemat-Nasser and Y. X. Wu, (to be published).
[4] S. Nemat-Nasser and C. Thomas, in *Electroactive Polymer (EAP) Actuators as Artificial Muscles—Reality, Potential and Challenges*, edited by Bar-Cohen, (SPIE, Bellingham, WA, 2001), Chap. 6, pp. 139–191.
[5] C. Heitner-Wirguin, J. Membr. Sci. **120**, 1 (1996).
[6] P. J. James, J. A. Elliott, T. J. McMaster, J. M. Newton, A. M. S. Elliott, S. Hanna, and M. J. Miles, J. Mater. Sci. **35**, 5111 (2000).
[7] S. Nemat-Nasser and N. Wong (unpublished).
[8] P. Millet, M. Pineri, and R. Durand, J. Appl. Electrochem. **19**, 162 (1989).
[9] P. Millet, R. Durand, E. Dartyge, G. Tourillon, and A. Fontaine, J. Electrochem. Soc. **140**, 1373 (1993).
[10] P. Millet, F. Andolfatto, and R. Durand, J. Appl. Electrochem. **25**, 227 (1995).
[11] P. Millet, J. Chem. Educ. **76**, 47 (1999).
[12] M. Shahinpoor and K. J. Kim (private communication).
[13] M. Shahinpoor and K. J. Kim, Proc. SPIE, 174 (2001).
[14] K. Onishi, S. Sewa, K. Asaka, N. Fujiwara, and K. Oguro, Electrochim. Acta **46**, 737 (2000).
[15] S. Nemat-Nasser, D. Lischer, J. McGee, S. Sarva, C. Thomas, and Y. X. Wu (to be published).
[16] A. Eisenberg, Macromolecules **3**, 147 (1970).
[17] A. Eisenberg and J.-S. Kim, in *Polymeric Materials Encyclopedia*, edited by Salamone, J. C., (CRC Press, Boca Raton, FL, 1996), pp. 3435–3454.
[18] T. D. Gierke, C. E. Munn, and P. N. Walmsley, J. Polym. Sci., Polym. Phys. Ed. **19**, 1687 (1981).
[19] W. Y. Hsu and T. D. Gierke, Macromolecules **13**, 198 (1982).
[20] K. A. Mauritz, J. Macromol. Sci. Rev. Macromol. Chem. C **28**, 65 (1988).
[21] T. Xue, J. S. Trent, and K. Osseo-Asare, J. Membr. Sci. **45**, 261 (1989).
[22] E. M. Lee, R. K. Thomas, A. N. Burgess, D. Y. S. Barnes, A. K. Oper, and A. R. Rennil, Macromolecules **25**, 3106 (1992).
[23] J. Y. Li and S. Nemat-Nasser, Mech. Mater. **32**, 303 (2000).
[24] S. Nemat-Nasser and J. Y. Li, J. Appl. Phys. **87**, 3321 (2000).
[25] A. Agmon, Chem. Phys. Lett. **244**, 456 (1995).
[26] N. Agmon, Isr. J. Chem. **39**, 493 (1999).
[27] R. Pomes, ''Theoretical studies of the Grotthuss mechanism in biological proton wires,'' Isr. J. Chem. **39**, 387 (1999).
[28] L. R. G. Treolar, *Physics of Rubber Elasticity* (Oxford University Press, New York, 1958).
[29] R. J. Atkin and N. Fox, *An Introduction to the Theory of Elasticity* (Longman, London, 1980).
[30] R. A. Robinson and R. H. Stokes, *Electrolyte Solutions*, 2nd (revised) ed. (Butterworths, London, 1965).
[31] O. D. Bonner, J. Am. Chem. Soc. **103**, 3262 (1981).
[32] S. Nemat-Nasser and M. Hori, *Micromechanics: Overall Properties of Heterogeneous Materials*, 2nd ed. (Elsevier, Amsterdam, 1999).
[33] Set $z=L$, $u_0=0$, $h=H$, $u=\dot{u}$, and $\varepsilon_{\max}=\dot{\varepsilon}_{\max}$ in Eq. (14), of S. Nemat-Nasser and C. Thomas in *Electroactive Polymer (EAP) Actuators as Artificial Muscles—Reality, Potentials and Challenges*, edited by Bar-Cohen (SPIE, Bellingham, WA, 2001), p. 157, where a derivation is sketched.
[34] N. Lakshminarayanaiah, *Transport Phenomena in Membranes* (Academic, New York, 1969).
[35] If Cap is the measured overall capacitance, then we set $\overline{\kappa}=2H$ Cap.
[36] In a recent report, Y. Xiao and K. Bhattacharya, Proc. SPIE **4329**, 292 (2001), the effects of the nonlinear terms of the equations given by Nemat-Nasser and Li (2000)[24] have been examined, without including the capacitive nature of the IPMC. This produced extremely small values for the length scale, denoted by ℓ in the present work. In their parametric simulations, however, the authors use large values for this length scale and set $\phi_0 F/(RT)$ (which is about 39 for $\phi_0=1$ V) equal to 1, rendering the results inappropriate for comparison with experimental data.
[37] Since the distribution of the volume fraction of water through the thickness changes with cation redistribution, C^- does not remain constant, as pointed out by Nemat-Nasser and Thomas (2001, p. 171, Eq. 27).[4] Indeed, since $(1+w)C^-$ is constant, being the anion charge density per unit volume of the dry membrane, we have $F\partial C^-/\partial x=-C^-F/(1+w)(\partial w/\partial x)$, which must be added to the expression inside the parentheses in Eq. (56). Furthermore, the gradient of w is proportional to the net charge distribution and is given by $\partial \ln(1+w)/\partial x=[1-A_0(C^+-C^-)]^{-1}A_0[\partial(C^+-C^-)/\partial x]$, where $A_0=18\times10^{-6}$ SN. Thus, the contribution to Eq. (56) due to the dependence of C^- on w is viewed to be small and has been neglected in the present analysis.